

## Nanothermometry

# [Ga<sup>3+</sup><sub>8</sub>Sm<sup>3+</sup><sub>2</sub>, Ga<sup>3+</sup><sub>8</sub>Tb<sup>3+</sup><sub>2</sub>] Metallacrowns are Highly Promising Ratiometric Luminescent Molecular Nanothermometers Operating at Physiologically Relevant Temperatures

Elvin V. Salerno,<sup>[a]</sup> Justyna Zeler,<sup>[b, c]</sup> Svetlana V. Eliseeva,<sup>\*,[d]</sup> Miguel A. Hernández-Rodríguez,<sup>[b]</sup> Albano N. Carneiro Neto,<sup>[b]</sup> Stéphane Petoud,<sup>\*,[d]</sup> Vincent L. Pecoraro,<sup>\*,[a]</sup> and Luís D. Carlos<sup>\*,[b]</sup>

**Abstract:** Nanothermometry is the study of temperature at the submicron scale with a broad range of potential applications, such as cellular studies or electronics. Molecular luminescent-based nanothermometers offer a non-contact means to record these temperatures with high spatial resolution and thermal sensitivity. A luminescent-based molecular thermometer comprised of visible-emitting Ga<sup>3+</sup>/Tb<sup>3+</sup> and Ga<sup>3+</sup>/Sm<sup>3+</sup> metallacrowns (MCs) achieved remarkable relative thermal sensitivity associated with very low temperature uncertainty of  $S_r = 1.9\%K^{-1}$  and  $\delta T < 0.045$  K, respectively, at 328 K, as an aqueous suspension of polystyrene nanobeads loaded with the corresponding MCs. To date, they are the ratiometric molecular nanothermometers offering the highest level of sensitivity in the physiologically relevant temperature range.

Nanothermometry is the analysis of the temperature of submicron systems. This domain of science offers potential applications in fields such as electronics,<sup>[1]</sup> microfluidics,<sup>[2]</sup> nanomedicine,<sup>[3]</sup> and cellular studies<sup>[4]</sup> where minimal spatial-sized thermometers are desired. Luminescence based thermometry correlates temperature with either emission intensity or emission lifetime changes of luminescent systems located in the studied environment. A low temperature uncertainty ( $\delta T$ ) and a high

relative thermal sensitivity of measurements ( $S_r$ ) are desirable properties.

Dual-centered ratiometric luminescent thermometry is a proven intensity-based method. In this technique, the intensity ratio ( $\Delta$ ) of two unique emitters' emission wavelengths provides a measurement of temperature with an internal calibration.<sup>[5]</sup> Molecular luminescence thermometry approaches what is perhaps the physical limit of attainable optical spatial resolution of temperature, restrained only by the diffraction limit of the optics used for detection.<sup>[6,7]</sup> It is difficult to generalize the parameters related to molecular thermometers, since while a system may excel in some respects it may be lacking in others. Molecular thermometers have been created using organic fluorescence dyes or transition metal complexes or clusters.<sup>[3,6,8-12]</sup> However, such systems have drawbacks since they usually exhibit limited photostability that depends on the intensity and duration of the light exposure, and can suffer from fluorescence intensity changes that are not related to variations of temperature but to modifications of pH, solvent viscosity or polarity, biological environment, or ionic strength. The wide emission bandwidths of organic reporters can complicate the interpretations of results in practical applications, and moreover, the luminescence lifetimes are most often used in the evaluation of temperature in such systems, with inherent drawbacks such as longer acquisition times and the requirement of rigorous post-processing data treatment as well as the inadequacy in mapping temperature gradients.<sup>[5]</sup>

Lanthanide-based nanothermometers<sup>[13]</sup> may derive their functionality from the temperature-dependent luminescence of lanthanide cations (Ln<sup>3+</sup>) in their compounds. Unique Ln<sup>3+</sup> photophysical properties originate from their core-like valence 4f electrons. These cations possess element-specific emission profiles with narrow bands the wavelengths of which are not affected by the experimental conditions. As most f-f transitions are forbidden, free Ln<sup>3+</sup> are very weakly absorbing resulting in low emission intensity. This limitation can be overcome through sensitization by an appropriate coordination environment.<sup>[14]</sup>


While thermometers incorporating Ln<sup>3+</sup> are relatively common among metal-organic frameworks (MOFs) and other solid-state compounds (e.g. inorganic nanoparticles),<sup>[15-18]</sup> examples of self-sensitized molecular-based Ln<sup>3+</sup> systems with thermometric properties are very scarce. Namely, such systems include: (i) a Eu<sup>3+</sup> thenoyltrifluoroacetate complex (EuTTA) embedded in a poly(methylmethacrylate) network which has a

[a] E. V. Salerno, Prof. Dr. V. L. Pecoraro  
Department of Chemistry, University of Michigan  
Ann Arbor, MI 48108 (USA)  
E-mail: vlpec@umich.edu

[b] Dr. J. Zeler, Dr. M. A. Hernández-Rodríguez, Dr. A. N. Carneiro Neto,  
Prof. Dr. L. D. Carlos  
Phantom-g, CICECO-Aveiro Institute of Materials, Department of Physics  
University of Aveiro, Campus de Santiago, Aveiro (Portugal)  
E-mail: lcarlos@ua.pt

[c] Dr. J. Zeler  
Faculty of Chemistry, University of Wrocław, Wrocław (Poland)

[d] Dr. S. V. Eliseeva, Prof. Dr. S. Petoud  
Centre de Biophysique Moléculaire  
CNRS, UPR 4301, 45071 Orléans Cedex 2 (France)  
E-mail: svetlana.eliseeva@cnrs-orleans.fr  
stephane.petoud@inserm.fr

 Supporting information and the ORCID identification number(s) for the author(s) of this article can be found under:  
<https://doi.org/10.1002/chem.202003239>

$\delta T$  of 0.3 K,<sup>[10]</sup> (ii) a dimeric Tb<sup>3+</sup> 1,1,1-trifluoroacetylacetonate with 2,2'-bipyrimidine (Tb<sub>2</sub>(bpm)(tfac)<sub>6</sub>) with an  $S_r = 5.9\%K^{-1}$  at 300 K,<sup>[19]</sup> and (iii) a Tb<sup>3+</sup>-Eu<sup>3+</sup> dyad with a  $\delta T$  of 1 K ( $S_r = 1.876\%K^{-1}$ ) at  $\approx 200$  K.<sup>[20]</sup> The EuTTA and Tb<sub>2</sub>(bpm)(tfac)<sub>6</sub> complexes possess respectable thermometric parameters, however, luminescent lifetimes were used for the determination of the relative temperatures which suffer from drawbacks such as instrumental complexity, inadequacy at mapping temperature gradients, and limited efficiency in dynamic measurements where the temperature changes are faster than the lifetime of the luminescent state of the corresponding Ln<sup>3+</sup>.<sup>[5]</sup> The Tb<sup>3+</sup>-Eu<sup>3+</sup> dyad, although notable for possessing a stoichiometric Tb-Eu ratio, operates optimally at ca. 200 K, a temperature that is not suitable for biological applications such as cellular temperature mapping. Therefore, there is a need to create ratiometric luminescent molecular thermometers that would overcome existing challenges and exhibit reliable thermometric parameters in the physiological range of temperatures while operating in biological conditions.

Herein we present a novel type of ratiometric luminescent nanothermometer based on the Ga<sub>8</sub>Ln<sub>2</sub>(salicylhydroximate)<sub>8</sub>(isophthalate)<sub>4</sub> metallacrown platform ([MC:Ln], Figure 1) using a 1:1 mixture of Ga<sub>8</sub>Tb<sub>2</sub> and Ga<sub>8</sub>Sm<sub>2</sub> molecules.<sup>[21]</sup> These macromolecules possess an organic framework which is templated by eight diamagnetic d<sup>10</sup> Ga<sup>3+</sup> and two Ln<sup>3+</sup>. This MC scaffold can sensitize the emission of different Ln<sup>3+</sup> in the visible and near-infrared (NIR) regions with remarkable luminescence intensities. We have previously demonstrated that this family of MCs has great potential for NIR cell imaging.<sup>[21]</sup> The luminescence properties and the temperature dependences have been studied here on 10 mg mL<sup>-1</sup> aqueous suspensions of 100 nm amino-functionalized polystyrene nanobeads loaded with corresponding MCs ([MC:Ln]@PS/NH<sub>2</sub>). Data are presented for the nanobeads loaded with mono-lanthanide complexes, that is, [MC:Sm]@PS/NH<sub>2</sub> and [MC:Tb]@PS/NH<sub>2</sub>, as well as for the 1:1 [MC:Sm]:[MC:Tb] mixed-lanthanide compound: [MC:Sm,Tb]@PS/NH<sub>2</sub>.

The excitation spectra of [MC:Tb]@PS/NH<sub>2</sub> and [MC:Sm]@PS/NH<sub>2</sub> upon monitoring the sharp emission band of the corresponding lanthanide cation (<sup>5</sup>D<sub>4</sub> → <sup>7</sup>F<sub>5</sub> (Tb<sup>3+</sup>, 545 nm) and <sup>4</sup>G<sub>5/2</sub>

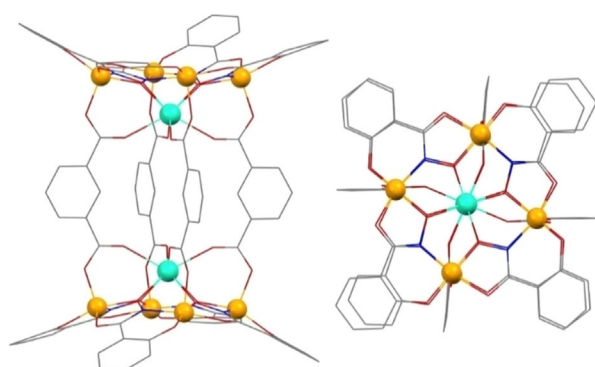


**Figure 1.** Structure of [MC:Ln] from the side (left) and top (right) views.<sup>[21]</sup> Color code: Ga, orange; Ln, green; O, red; N, blue; C, grey. Solvents, counter cations, and hydrogen atoms are omitted for clarity. CCDC Identifier: FELPUK, the structure was solved for the Dy analogue.

→ <sup>6</sup>H<sub>7/2</sub> (Sm<sup>3+</sup>, 600 nm)) were collected at ambient temperature. Results were compared to the corresponding excitation spectra of the [MC:Sm,Tb]@PS/NH<sub>2</sub> upon monitoring the <sup>5</sup>D<sub>4</sub> → <sup>7</sup>F<sub>6</sub> (Tb<sup>3+</sup>, 490 nm) and the <sup>4</sup>G<sub>5/2</sub> → <sup>6</sup>H<sub>9/2</sub> (Sm<sup>3+</sup>, 650 nm) transitions, respectively. All excitation spectra show a series of broad bands located in the 250–370 nm wavelength range (Figure S1 a,b). The high similarities between these different excitation spectra indicate that the electronic states located in the common chromophoric part of the MC scaffold in [MC:Ln] are used to sensitize Tb<sup>3+</sup> and Sm<sup>3+</sup> via an antenna effect.<sup>[14]</sup>

Emission spectra of [MC:Sm]@PS/NH<sub>2</sub>, [MC:Tb]@PS/NH<sub>2</sub> and [MC:Sm,Tb]@PS/NH<sub>2</sub> collected upon 340 nm excitation at room temperature show the corresponding typical emission bands of Tb<sup>3+</sup> (490 nm [<sup>5</sup>D<sub>4</sub> → <sup>7</sup>F<sub>6</sub>], 545 nm [<sup>5</sup>D<sub>4</sub> → <sup>7</sup>F<sub>5</sub>], 570 nm [<sup>5</sup>D<sub>4</sub> → <sup>7</sup>F<sub>4</sub>], and 620 nm [<sup>5</sup>D<sub>4</sub> → <sup>7</sup>F<sub>6</sub>]) and of Sm<sup>3+</sup> (562 nm [<sup>4</sup>G<sub>5/2</sub> → <sup>6</sup>H<sub>5/2</sub>], 600 nm [<sup>4</sup>G<sub>5/2</sub> → <sup>6</sup>H<sub>7/2</sub>], 645 nm [<sup>4</sup>G<sub>5/2</sub> → <sup>6</sup>H<sub>9/2</sub>], and 700 nm [<sup>4</sup>G<sub>5/2</sub> → <sup>6</sup>H<sub>11/2</sub>]). Partial overlaps can be observed between the emission bands related to the <sup>5</sup>D<sub>4</sub> → <sup>7</sup>F<sub>5</sub> (Tb<sup>3+</sup>) and <sup>4</sup>G<sub>5/2</sub> → <sup>6</sup>H<sub>5/2</sub> (Sm<sup>3+</sup>) transitions, and the <sup>5</sup>D<sub>4</sub> → <sup>7</sup>F<sub>4</sub> (Tb<sup>3+</sup>) and <sup>4</sup>G<sub>5/2</sub> → <sup>6</sup>H<sub>7/2</sub> (Sm<sup>3+</sup>) transitions (Figure S2).

The study of the temperature changes through the emission intensity of [MC:Sm,Tb]@PS/NH<sub>2</sub> in the physiological range (ca. 298–328 K, 25–55 °C) was performed under 340 nm excitation (Figure 2). The integrated intensities of the emission bands related to the <sup>5</sup>D<sub>4</sub> → <sup>7</sup>F<sub>6,3</sub> transitions of Tb<sup>3+</sup> and the <sup>4</sup>G<sub>5/2</sub> → <sup>6</sup>H<sub>9/2</sub> transition of Sm<sup>3+</sup> were monitored (Figure 3a). The luminescence intensities collected on two Tb<sup>3+</sup> transitions (<sup>5</sup>D<sub>4</sub> → <sup>7</sup>F<sub>6,3</sub>) remain the same or show a slight increase from 298 K to 303 K and are followed by a significant decrease upon further heating up to 328 K. The intensity of the Sm<sup>3+</sup>-based <sup>4</sup>G<sub>5/2</sub> → <sup>6</sup>H<sub>9/2</sub> transition is approximately constant across the temperature range examined (Figure 3a).

The relationship between Tb<sup>3+</sup> and Sm<sup>3+</sup> integrated emission intensities can be used as ratio-thermometric measurements in order to evaluate the temperature of the [MC:Sm,Tb]@PS/NH<sub>2</sub> environment. We define  $\Delta_1 = I_D/I_G$  where  $I_G$

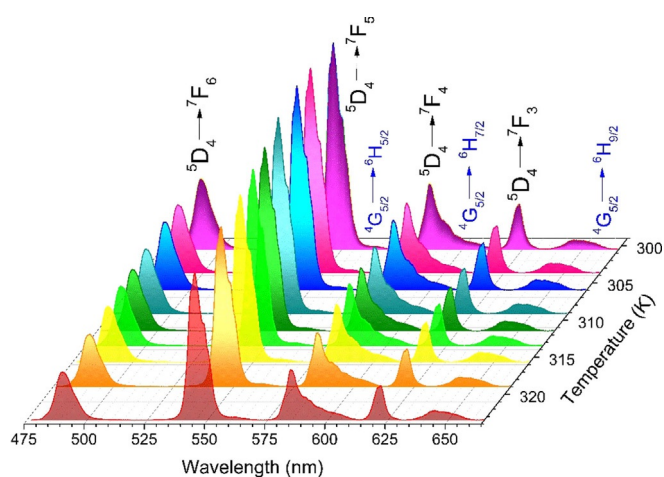


**Figure 2.** Luminescence intensities collected on 10 mg mL<sup>-1</sup> aqueous suspension of [MC:Sm,Tb]@PS/NH<sub>2</sub> beads upon excitation at 340 nm at temperatures ranging from 298 to 328 K. The transitions are labelled in black for Tb<sup>3+</sup> and in blue for Sm<sup>3+</sup>.

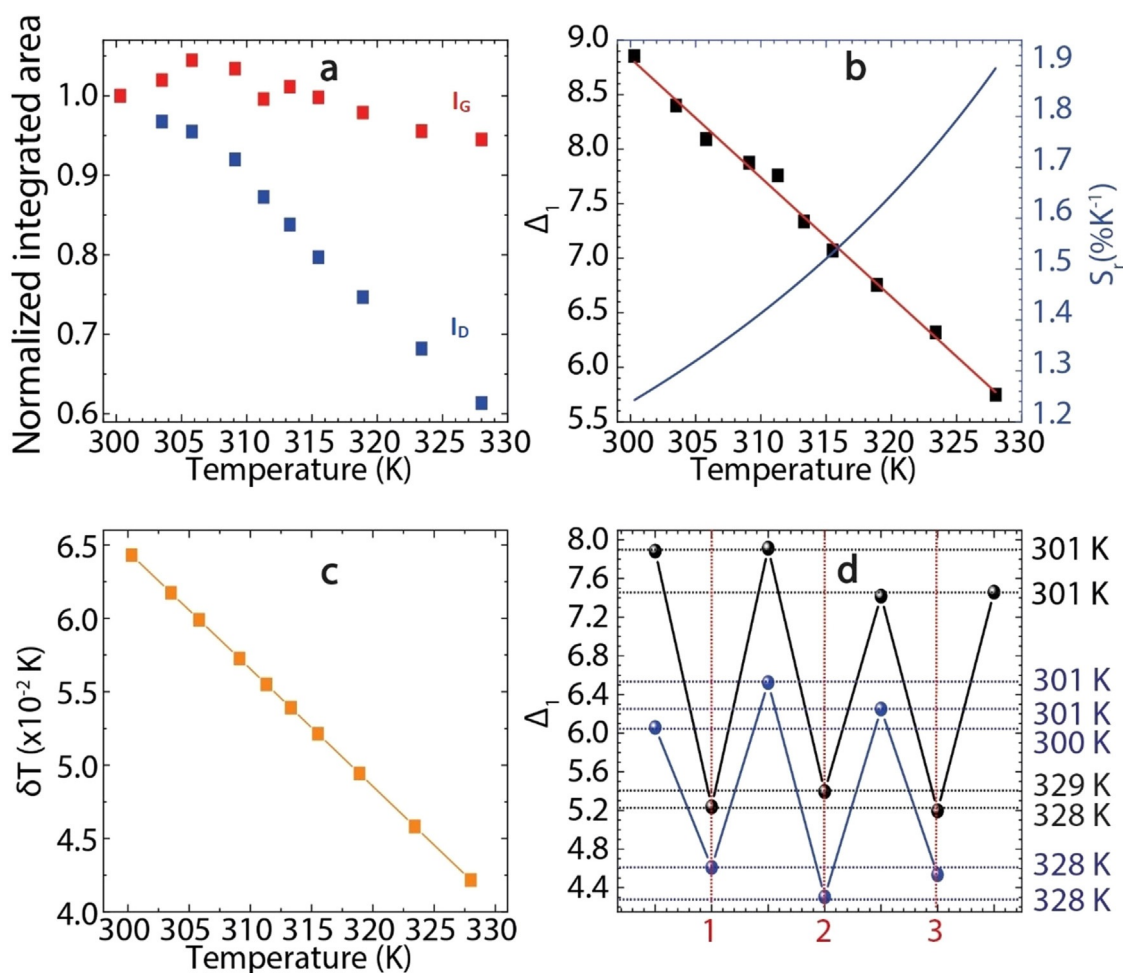


**Figure 3.** Thermometric behavior of the 10 mg mL<sup>-1</sup> aqueous suspension of [MC:Sm,Tb]@PS/NH<sub>2</sub> beads upon excitation at 340 nm in the temperature range 298–328 K. (a) Temperature evolution of  $I_G$  ( $\text{Sm}^{3+}$ ,  ${}^4\text{G}_{5/2} \rightarrow {}^6\text{H}_{9/2}$ ) (red) and  $I_D$  ( $\text{Tb}^{3+}$ ,  ${}^5\text{D}_4 \rightarrow {}^7\text{F}_6$ ) (blue) from 298 K to 328 K. (b) The experimental thermometric parameter  $\Delta_1$  is given in black, while the fitted  $\Delta_1$  is given by the red curve and  $S_r$  is shown by the blue curve. (c) The temperature uncertainty,  $\delta T$ , was calculated using the thermometric parameter  $\Delta_1$ . (d) The temperature cycling experiment was carried out twice with an intermediary period of 3 months. The black and blue dots represent the first and second experiments, respectively, showing reversibility around 99.89% and 99.92% in 3 consecutive cycles.

and  $I_D$  are the integrated areas of the  ${}^4\text{G}_{5/2} \rightarrow {}^6\text{H}_{9/2}$  ( $\text{Sm}^{3+}$ ) and  ${}^5\text{D}_4 \rightarrow {}^7\text{F}_6$  ( $\text{Tb}^{3+}$ ) transitions, respectively. The temperature evolution of  $\Delta_1$  from 298 K to 328 K can be fitted as a linear function is shown in Figure 3b.

From this fitting process, the relative sensitivity ( $S_r$ ) can be estimated according to the Equation (1):

$$S_r = \frac{1}{\Delta_1} \frac{\partial \Delta_1}{\partial T} \quad (1)$$

Temperature uncertainties ( $\delta T$ , Figure 3c) were calculated as:

$$\delta T = \frac{1}{S_r} \frac{\partial \Delta_1}{\Delta_1} \quad (2)$$

in which  $\delta \Delta_1$  is derived from the experimental uncertainty.<sup>[5]</sup> This system demonstrates a  $\delta T < 0.07$  K throughout the examined range and a maximum  $S_r = 1.9\%$  K<sup>-1</sup> at 328 K (Figure 3b). The thermometric behavior is similar whether using the  ${}^5\text{D}_4 \rightarrow {}^7\text{F}_3$  or  ${}^5\text{D}_4 \rightarrow {}^7\text{F}_6$   $\text{Tb}^{3+}$  transition (Figures S4, S5 and Table S1), however the  ${}^5\text{D}_4 \rightarrow {}^7\text{F}_6$  emission is used here due to an overall lower dispersion of  $\delta T$ .

To evaluate the mechanisms of nanothermometer action, the luminescence lifetimes and intensities of [MC:Sm]@PS/NH<sub>2</sub>, [MC:Tb]@PS/NH<sub>2</sub>, and [MC:Sm,Tb]@PS/NH<sub>2</sub> were measured as a function of temperature. Since the integrated intensities of  $\text{Sm}^{3+}$  bands are fairly similar when comparing the [MC:Sm]@PS/NH<sub>2</sub> and [MC:Sm,Tb]@PS/NH<sub>2</sub> (Figure 4), there is no significant energy transfer from  $\text{Tb}^{3+}$  to  $\text{Sm}^{3+}$ , corroborated by theoretical calculations (Ln-to-Ln energy transfer section in the Supporting Information).

Experimental emission decays of  $\text{Sm}^{3+}$  measured on the  ${}^4\text{G}_{5/2}$  level on [MC:Sm]@PS/NH<sub>2</sub> and [MC:Sm,Tb]@PS/NH<sub>2</sub> are both best fitted with bi-exponential functions resulting in individual lifetime values that can be considered as temperature independent (Figure S6, Tables S3, S4).

The temperature dependences of integrated intensities of  $\text{Tb}^{3+}$  emission bands for [MC:Tb]@PS/NH<sub>2</sub> and [MC:Sm,Tb]@PS/NH<sub>2</sub> samples are comparable, however changes are more significant for the former sample (Figure 4). There is a notable decrease in integrated emissive intensity as temperature increases. There are two distinct observed luminescence lifetimes of

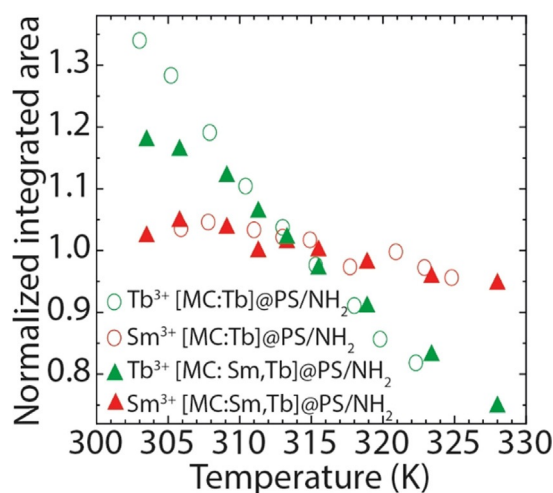


**Figure 4.** Integrated emission signals of  $\text{Sm}^{3+}$  ( ${}^4\text{G}_{5/2} \rightarrow {}^6\text{H}_{9/2}$ ) and  $\text{Tb}^{3+}$  ( ${}^5\text{D}_4 \rightarrow {}^7\text{F}_6$ ) in  $[\text{MC:Sm}]@\text{PS}/\text{NH}_2$ ,  $[\text{MC:Tb}]@\text{PS}/\text{NH}_2$ , and  $[\text{MC:Sm,Tb}]@\text{PS}/\text{NH}_2$  samples normalized to the average integrated intensity. The emission intensities are very similar between the mixed and mono-lanthanide  $\text{Tb}^{3+}/\text{Sm}^{3+}$  samples.

the  $\text{Tb}^{3+}$  excited  ${}^5\text{D}_4$  level (Figure S7 and Table S5, S6). Globally, we can notice a decrease in observed luminescence lifetimes as temperature increases.

Because the MCs are embedded in 100 nm polystyrene beads, they may experience different environments that may induce complex interactions. More specifically, we must take into account that MCs located in the core of the beads have less motional freedom and are more protected from interactions with solvent molecules than those located closer to the surface. This could explain why luminescence decays of  ${}^4\text{G}_{5/2}$  and  ${}^5\text{D}_4$  emitting levels are biexponential. Indeed, luminescence decays are monoexponential for the  $\text{Sm}^{3+}$  ( $\tau_{\text{obs}} = 117(1) \mu\text{s}$ ) and  $\text{Tb}^{3+}$  ( $\tau_{\text{obs}} = 1410(1) \mu\text{s}$ ) MCs in the solid-state.<sup>[21]</sup> These observed solid-state lifetimes are longer but close to the corresponding “longer” lifetime values found for aqueous suspension of  $[\text{MC:Tb}]@\text{PS}/\text{NH}_2$ ,  $[\text{MC:Sm}]@\text{PS}/\text{NH}_2$ , and  $[\text{MC:Sm,Tb}]@\text{PS}/\text{NH}_2$  beads.<sup>[19]</sup>

This nonradiative relaxation is derived from back-transfer to the triplet state of the salicylhydroxamate ligand. The ligand triplet state was previously determined in the solid-state as  $E_T^* = 21,980 \text{ cm}^{-1}$  by the recording of phosphorescence spectra.<sup>[21]</sup> Intramolecular energy transfers (IET) from ligands states to the  $\text{Tb}^{3+}$  in  $[\text{MC:Tb}]@\text{PS}/\text{NH}_2$  were estimated using the theory introduced by Malta et al.<sup>[22,23]</sup> The theoretical analysis (Supporting Information) indicates that the sensitization energy comes from the singlet state instead of the triplet one. This process is associated with the energetic positions of these donor states. The  $T_1$  state is not in a favorable energetic position (the best acceptor state is  ${}^7\text{F}_6 \rightarrow {}^5\text{D}_4$  with  $\Delta E = 1536 \text{ cm}^{-1}$ ) while  $S_1$  is in good resonance with three acceptor states:  ${}^7\text{F}_6 \rightarrow {}^5\text{H}_7$  ( $\Delta E = -129 \text{ cm}^{-1}$ ),  ${}^7\text{F}_5 \rightarrow {}^5\text{H}_6$  ( $\Delta E = 407 \text{ cm}^{-1}$ ), and  ${}^7\text{F}_5 \rightarrow {}^5\text{H}_5$  ( $\Delta E = -469 \text{ cm}^{-1}$ ). Using the selection rules on the quantum number  $J$ , the last three are allowed for the exchange mechanism while  ${}^7\text{F}_6 \rightarrow {}^5\text{D}_4$  is forbidden by the same mechanism. The  ${}^7\text{F}_5$  level is also considered in the calculations due to an abnormally longer lifetime and an important role in the IET pro-

cess.<sup>[24–27]</sup> Once the energy populates  $\text{Tb}^{3+}$  electronic states by the ligand's  $S_1$  level, the population in higher  $\text{Tb}^{3+}$  states tends to decay non-radiatively until reaching the emissive level of  $\text{Tb}^{3+}$  ( ${}^5\text{D}_4$ ). In this process, non-radiative energy losses occur in intermediate energy levels through a backward energy transfer to  $T_1$ . This process happens when populations reach the  ${}^5\text{G}_5$  and  ${}^5\text{G}_6$  levels, donating back the energy to the ligand  $T_1$  state with a rate in the order of  $8 \times 10^6 \text{ s}^{-1}$  in pathways involving the  ${}^5\text{G}_{5,6} \rightarrow {}^7\text{F}_{5,6}$  transitions (which is also dominated by the exchange mechanism). Indeed, another study demonstrated that the  $\text{Tb}^{3+}$ -ligand triplet energy transfer is an effective channel for  $\text{Tb}^{3+}$  thermal emission dependence.<sup>[19]</sup>  $\text{Sm}^{3+}$ , with a lower energy emissive state ( ${}^4\text{G}_{5/2} \rightarrow {}^6\text{H}_{5/2}$ ), having a larger energy difference with the ligand triplet state with a forward IET rate of  $1.9 \times 10^{10} \text{ s}^{-1}$ , is therefore less prone to back energy transfer ( $\approx 70 \text{ s}^{-1}$ ) thus explaining its temperature-constant luminescence lifetimes.

The performance of this novel generation of  $[\text{MC:Sm,Tb}]@\text{PS}/\text{NH}_2$  thermometer as an aqueous suspension has been compared to other nanothermometers incorporating two different visible-emitting  $\text{Ln}^{3+}$  ions (Table S2). The  $[\text{MC:Sm,Tb}]@\text{PS}/\text{NH}_2$  beads analyzed in the physiological temperature range exhibit generally comparable performances to most of solid-state ratiometric thermometers (Table S2). Some systems, however, including MOFs<sup>[28,29]</sup> and nanoparticles,<sup>[30]</sup> offer higher sensitivity, but they are bulk solid-state materials that require proper miniaturization and surface functionalization before being used for biological applications. Moreover, in such materials thermal sensing mechanism is usually governed by the energy transfer between different  $\text{Ln}^{3+}$ . The described ratiometric thermometer was prepared as  $[\text{MC:Sm,Tb}]$  within  $\text{PS}/\text{NH}_2$  nanobeads to confer biocompatibility, however, we confirmed that sensitization and emission processes in this system follow the behaviors of discrete molecular units. This is an innovative approach to create biologically compatible  $\text{Ln}^{3+}$ -based thermometers and provides another avenue for future applications such as cellular thermal imaging.

In summary, the mixed  $\text{Sm}^{3+}$ - $\text{Tb}^{3+}$   $[\text{MC:Sm,Tb}]@\text{PS}/\text{NH}_2$  system behaves as a ratiometric luminescent molecular thermometer with  $S_r$  of  $1.9\% \text{ K}^{-1}$  at 328 K and is an effective nanothermometer for the physiological temperature regime with  $\delta T$  measured  $< 0.045 \text{ K}$  at 328 K. This is among the most sensitive visible emission-based nanothermometers of any type in the physiological range and is especially notable for being molecular-based and water-stable. These properties are highly promising in respect to temperature sensitivity and precision while opening the possibility for enhanced spatial resolution. Taking into account that several families of photostable, visible- and NIR-emitting  $\text{Ln}^{3+}$ -based MCs have been created,<sup>[21,31–33]</sup> future work will examine in greater details the thermometric potential of these molecules following the strategy suggested herein.

This study performed with MCs constitutes a broader demonstration of the effectiveness of a  $\text{Ln}^{3+}$ -based molecular approach to nanothermometry. As opposed to  $\text{Ln}^{3+}$ -doped solid-state compounds, molecules possess a uniform environment surrounding each luminescent cation. This can lead to more



consistent emitting processes and thus reduce uncertainty related to each measurement.

In addition to the nanometer sizes of these novel thermometers, MC molecules are also relatively easy to modify using the wealth of chemical techniques with a limited synthetic effort. Such high level of tunability could lead to the improvement of Ln<sup>3+</sup> sensitization and thermometric sensitivity,<sup>[34]</sup> control the regions of thermometric effectiveness, enhance solubility, or even promote cellular uptake or binding via appendages such as antibodies.<sup>[35]</sup>

## Acknowledgements

This work was developed within the scope of the project CICECO-Aveiro Institute of Materials, UIDB/50011/2020, financed by Portuguese funds through the FCT/MEC and when appropriate co-financed by FEDER under the PT2020 Partnership Agreement. Financial support from the European Union's Horizon 2020 FET Open programme under grant agreement no. 801305 is also acknowledged. A.N.C.N. thanks SusPhotoSolutions project, CENTRO-01-0145-FEDER-000005, Portugal for his grant. The authors acknowledge R.A.S. Ferreira (University of Aveiro) for her help with the luminescence lifetime measurements and analysis. V.L.P. thanks NSF grant CHE-1664964. E.V.S. thanks the Rackham Graduate School for international travel funding as well as NSF grant DGE-1256260. We thank Le Studium Loire Valley Institute for Advanced Studies for the award of a LE STUDIUM Research Consortium "Lanthanide-Based Agents for Sensitive and Selective Near-Infrared Imaging of Living Biological Systems". S.P. acknowledges support from the Institut National de la Santé et de la Recherche Médicale (INSERM). The work in Orléans has been supported by la Ligue Contre le Cancer, La Région Centre and Réseau Molécules Marines, Métabolisme & Cancer of Cancéropôle Grand Ouest.

## Conflict of interest

The authors declare no conflict of interest.

**Keywords:** lanthanides • luminescence • metallacrowns • nanoparticles • nanothermometry

- [1] C. D. S. Brites, P. P. Lima, N. J. O. Silva, A. Millán, V. S. Amaral, F. Palacio, L. D. Carlos, *Front. Chem.* **2013**, *1*, 1–6.
- [2] E. M. Graham, K. Iwai, S. Uchiyama, A. Prasanna De Silva, S. W. Magennis, A. C. Jones, *Lab Chip* **2010**, *10*, 1267–1273.
- [3] L. M. Maestro, P. Haro-Gonzalez, M. C. I. la Cruz, F. Sanz-Rodríguez, A. Juarranz, J. G. Sole, D. Jaque, *Nanomedicine* **2013**, *8*, 379–388.
- [4] S. Arai, M. Suzuki, S.-J. Park, J. S. Yoo, L. Wang, N.-Y. Kang, H.-H. Ha, Y.-T. Chang, *Chem. Commun.* **2015**, *51*, 8044–8047.
- [5] C. D. S. Brites, A. Millán, L. D. Carlos in *Handbook on the Physics and Chemistry of Rare Earths* (Eds.: J.-C. G. Bünzli, V. K. Pecharsky), Elsevier, Amsterdam, **2016**, pp. 339–427.
- [6] M. Quintanilla, L. M. Liz-Marzán, *Nano Today* **2018**, *19*, 126–145.
- [7] Editorial, *Nat. Photonics* **2009**, *3*, 361.

- [8] D. Cauzzi, R. Pattacini, M. Delferro, F. Dini, C. Di Natale, R. Paolesse, S. Bonacchi, M. Montalti, N. Zaccheroni, M. Calvaresi, F. Zerbetto, L. Prodi, *Angew. Chem. Int. Ed.* **2012**, *51*, 9662–9665; *Angew. Chem.* **2012**, *124*, 9800–9803.
- [9] F. Vetrone, R. Naccache, A. Zamarrón, A. J. De La Fuente, F. Sanz-Rodríguez, L. M. Maestro, E. M. Rodríguez, D. Jaque, J. G. Sole, J. A. Capobianco, *ACS Nano* **2010**, *4*, 3254–3258.
- [10] K. Oyama, M. Takabayashi, Y. Takei, S. Arai, S. Takeoka, S. Ishiwata, M. Suzuki, *Lab Chip* **2012**, *12*, 1591–1593.
- [11] H. Wang, D. Zhao, Y. Cui, Y. Yang, G. Qian, *J. Solid State Chem.* **2017**, *246*, 341–345.
- [12] A. V. Shamsieva, I. E. Kolesnikov, I. D. Strel'nik, T. P. Gerasimova, A. A. Kalinichev, S. A. Katsyuba, E. I. Musina, E. Lähderanta, A. A. Karasik, O. G. Sinyashin, *J. Phys. Chem. C* **2019**, *123*, 25863–25870.
- [13] C. D. S. Brites, S. Balabhadra, L. D. Carlos, *Adv. Opt. Mater.* **2019**, *7*, 1801239.
- [14] J.-C. G. Bünzli, *Coord. Chem. Rev.* **2015**, *293*, 19–47.
- [15] Y. Zhou, B. Yan, F. Lei, *Chem. Commun.* **2014**, *50*, 15235–15238.
- [16] Z. Wang, D. Ananias, A. Carné-Sánchez, C. D. S. Brites, I. Imaz, D. Maspocho, J. Rocha, L. D. Carlos, *Adv. Funct. Mater.* **2015**, *25*, 2824–2830.
- [17] M. Quintanilla, A. Benayas, R. Naccache, F. Vetrone in *Thermometry at the Nanoscale: Techniques and Selected Applications* (Eds.: L. D. Carlos, F. Palacio), Royal Society Of Chemistry, Cambridge, **2016**, pp. 124–166.
- [18] C. D. S. Brites, P. P. Lima, N. J. O. Silva, A. Millán, V. S. Amaral, F. Palacio, L. D. Carlos, *Nanoscale* **2013**, *5*, 7572–7580.
- [19] D. A. Gállico, R. Marin, G. Brunet, D. Errulat, E. Hemmer, F. A. Sigoli, J. O. Moilanen, M. Murugesu, *Chem. Eur. J.* **2019**, *25*, 14625–14637.
- [20] G. Bao, K. L. Wong, D. Jin, P. A. Tanner, *Light Sci. Appl.* **2018**, *7*, 96.
- [21] T. N. Nguyen, C. Y. Chow, S. V. Eliseeva, E. R. Trivedi, J. W. Kampf, I. Martinić, S. Petoud, V. L. Pecoraro, *Chem. Eur. J.* **2018**, *24*, 1031–1035.
- [22] O. L. Malta, *J. Lumin.* **1997**, *71*, 229–236.
- [23] A. N. Carneiro Neto, E. E. S. Teotonio, G. F. de Sá, H. F. Brito, J. Legendziejewicz, L. D. Carlos, M. C. F. C. Felinto, P. Gawryszewska, R. T. Moura, Jr., R. L. Longo, W. M. Faustonp, O. L. Malta in *Handbook on the Physics and Chemistry of Rare Earths* (Eds.: J.-C. G. Bünzli, V. K. Pecharsky), Elsevier, Amsterdam, **2019**, pp. 55–162.
- [24] A. S. Souza, L. A. Nunes, M. C. F. C. Felinto, H. F. Brito, O. L. Malta, *J. Lumin.* **2015**, *167*, 167–171.
- [25] U. N. Roy, R. H. Hawrami, Y. Cui, S. Morgan, A. Burger, K. C. Mandal, C. C. Noblitt, S. A. Speakman, K. Rademaker, S. A. Payne, *Appl. Phys. Lett.* **2005**, *86*, 151911.
- [26] E. Kasprzycka, A. N. Carneiro Neto, V. A. Trush, L. Jerzykiewicz, V. M. Amirkhanov, O. L. Malta, J. Legendziejewicz, P. Gawryszewska, *J. Rare Earths* **2020**, *38*, 552–563.
- [27] K. Rademaker, W. F. Krupke, R. H. Page, S. A. Payne, K. Petermann, G. Huber, A. P. Yelissev, L. I. Isaenko, U. N. Roy, A. Burger, *J. Opt. Soc. Am. B* **2004**, *21*, 2117.
- [28] D. Zhao, J. Zhang, D. Yue, X. Lian, Y. Cui, Y. Yang, G. Qian, *Chem. Commun.* **2016**, *52*, 8259–8262.
- [29] L. Zhang, Y. Xie, T. Xia, Y. Cui, Y. Yang, G. Qian, *J. Rare Earths* **2018**, *36*, 561–566.
- [30] E. C. Ximendes, U. Rocha, T. O. Sales, N. Fernández, F. Sanz-Rodríguez, I. R. Martín, C. Jacinto, D. Jaque, *Adv. Funct. Mater.* **2017**, *27*, 1702249.
- [31] E. R. Trivedi, S. V. Eliseeva, J. Jankolovits, M. M. Olmstead, S. Petoud, V. L. Pecoraro, *J. Am. Chem. Soc.* **2014**, *136*, 1526–1534.
- [32] C. Y. Chow, S. V. Eliseeva, E. R. Trivedi, T. N. Nguyen, J. W. Kampf, S. Petoud, V. L. Pecoraro, *J. Am. Chem. Soc.* **2016**, *138*, 5100–5109.
- [33] I. Martinić, S. V. Eliseeva, T. N. Nguyen, V. L. Pecoraro, S. Petoud, *J. Am. Chem. Soc.* **2017**, *139*, 8388–8391.
- [34] C. D. S. Brites, P. P. Lima, L. D. Carlos, *J. Lumin.* **2016**, *169*, 497–502.
- [35] R. Zhang, X. Qin, F. Kong, P. Chen, G. Pan, *Drug Delivery* **2019**, *26*, 328–342.

Manuscript received: July 9, 2020

Accepted manuscript online: July 14, 2020

Version of record online: September 29, 2020